Homogeneous Electrocatalytic Reduction of CO_2 by a CrN_3O Complex: Electronic Coupling with Redox-Active Terpyridine Fragment Favors Selectivity for CO

Amelia G. Reid,[†] Shelby L. Hooe,[†] Juan J. Moreno, Diane A. Dickie, and Charles W. Machan*

[†] - equal contributors; * - machan@virginia.edu; ORCID 0000-0002-5182-1138

A.G.R. ORCID: 0000-0002-2868-4091; S.L.H. ORCID 0000-0002-6991-2273; J.J.M. ORCID 0000-0003-1809-6170; D.A.D. ORCID 0000-0003-0939-3309

Department of Chemistry, University of Virginia, PO Box 400319, Charlottesville, VA 22904-4319

Abstract. Electrocatalyst design and optimization strategies continue to be an active area of research interest for the applied use of renewable energy resources. The electrocatalytic conversion of CO_2 is an attractive approach in this context, because of the added potential benefit of addressing its rising atmospheric concentrations. In previous experimental and computational studies, we have described the mechanism of the first molecular Cr complex capable of electrocatalytically reducing CO_2 to CO in the presence of an added proton donor, which contained a redox-active 2,2'-bipyridine (bpy) fragment, CrN_2O_2. The high selectivity for CO in the bpy-based system was dependent on a delocalized Cr(II)(bpy$^{\bullet-}$) active state. Subsequently, we became interested in exploring how expanding the polypyridyl ligand core would impact selectivity and activity during electrocatalytic CO_2 reduction. Here, we report a new CrN_3O catalyst, Cr(tpy^{tbu}pho)Cl_2 **1**, where 2-([2,2':6',2"-terpyridin]-6-yl)-4,6-di-tert-butylphenolate = [tpy^{tbu}pho]$^-$, which reduces CO_2 to CO with almost quantitative selectivity *via* a different mechanism than our previously reported Cr(^{tbu}dhbpy)Cl(H_2O) catalyst. Computational analyses indicate that although the stoichiometry of both reactions is identical, changes in the observed rate law are the combined result of a decrease in intrinsic ligand charge (L_3X vs L_2X_2) and an increase in ligand redox activity, which result in increased electronic coupling between the doubly reduced tpy fragment of the ligand and the Cr(II) center. The strong electronic coupling enhances the rate of protonation and subsequent C–OH bond

cleavage, resulting in CO_2 binding becoming the rate-determining step, which is an uncommon mechanism during protic CO_2 reduction.

Introduction

Rising concerns over increasing energy demands and global climate change have led to continued interest in the development of molecular catalysts capable of interconverting electrical and chemical energy.[1-3] Specifically, the electrocatalytic reduction of carbon dioxide (CO_2) to carbon monoxide (CO) using renewable energy[4-6] represents a potentially valuable pathway to the synthesis of liquid fuels via the Fischer-Tropsch process,[7] in the manufacturing of acetic acid,[8] and in hydroformylation reactions.[9] In homogeneous electrocatalysis for CO_2 reduction, the Cr/Mo/W triad is underrepresented,[4-6] with a limited number of reports of systems which are electrochemically or electrocatalytically active, few of which exhibit stability during electrolysis.[10-17]

Previously we reported the first homogeneous Cr electrocatalyst for quantitative CO_2 reduction to CO, Cr(^{tbu}dhbpy)Cl(H_2O), where 6,6′-di(3,5-di-tert-butyl-2-phenolate)-2,2′-bipyridine = [^{tbu}dhbpy]$^{2-}$.[18-20] We proposed a catalytic mechanism for the Cr(^{tbu}dhbpy)Cl(H_2O) catalyst whereby C–OH bond cleavage was the rate-determining step, based on mechanistic and computational studies. The noteworthy kinetic selectivity of this complex for CO was ascribed to the electronic structure of the catalytically active species: a square planar [Cr(II)(^{tbu}dhpy$^{\bullet}$)]$^{-}$ species (**Figure 1**) that exhibited anti-ferromagnetic coupling between a bpy-based radical anion and the Cr(II) center (S = 3/2). Based on previous reports about the role of electronic coupling in driving selectivity,[21-27] we reasoned that the redox activity of our bpy-based ligand could be translated to expanded polypyridyl ligand frameworks to examine how electronic coupling between Cr and the reduced ligand frameworks impacts catalytic performance. This was motivated by the known role

of electronic coupling between 2,2′:6′,2″-terpyridine (tpy) fragments or 2,2′:6′,2″:6″,2‴-quaterpyridine (qpy) and later transition metals like Fe[23-24, 27] or Co[27] in achieving high selectivity and activity at low overpotentials (η).

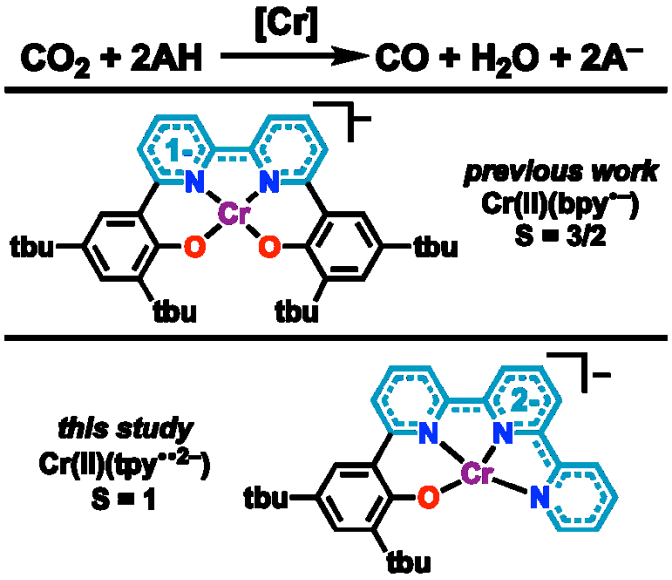

Figure 1. A comparison of the electronic structure of the active states for bpy- and tpy-based Cr complexes capable of mediating homogeneous electrocatalytic CO_2 reduction to CO.

Here we present a new molecular Cr catalyst, Cr(tpy^{tbu}pho)Cl_2 **1**, where 2-([2,2':6',2"-terpyridin]-6-yl)-4,6-di-tert-butylphenolate = [tpy^{tbu}pho]$^-$, which exhibits activity for CO_2 reduction to CO via a different mechanism relative to our initial Cr(^{tbu}dhbpy)Cl(H_2O) catalyst. Experimental and computational analyses reveal the new Cr(tpy^{tbu}pho)Cl_2 **1** electrocatalyst operates with important differences in the overall mechanism which arise from the expanded redox activity of the tpy fragment relative to bpy, achieving an active state best described as [Cr(II)(tpy^{tbu}pho$^{••}$)]$^-$ (**Figure 1**). Interestingly, these results also reveal that the charge of the supporting ligand plays an important role, since the benefit of expanded redox activity in [tpy^{tbu}pho]$^-$ appears to be balanced by the shift from a L_2X_2 coordination environment to L_3X. This study suggests that Cr electrocatalysts for CO_2 reduction can benefit from ligand design strategies that have previously been explored only for later transition metals.[23-24, 27]

Results and Discussion

The synthesis of 2-([2,2':6',2"-terpyridin]-6-yl)-4,6-di-tert-butylphenol, [tpy^{tbu}phoH]^{0}, was achieved via an initial coupling of 2,6-dibromopyridine to 2,2'-bipyridine to make 6-bromo-2,2':6',2"-terpyridine.[28] Subsequent microwave-assisted Suzuki-type cross-coupling of 6-bromo-2,2':6',2"-terpyridine with (3,5-di-*tert*-butyl-2-hydroxy-phenyl)boronic acid[18] produced [tpy^{tbu}pho(H)]^{0} in high yield. The Cr(tpy^{tbu}pho)Cl$_2$ **1** complex was synthesized in a similar manner to our previous report (see **SI: Materials and Methods**).[18] Both [tpy^{tbu}pho(H)]^{0} and **1** were characterized via HRMS and EA as well as NMR and UV-vis spectroscopies (SI **Materials and Methods** Section, **Table S2**, and **Figures S1-S5**). The proposed molecular connectivity was supported by structural data obtained from single-crystal X-ray diffraction studies (**Figure 2**).

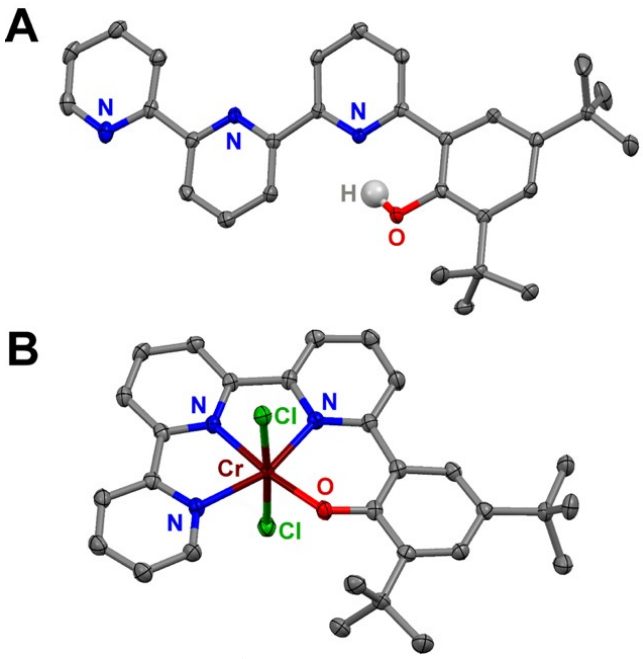

Figure 2. (**A**) Molecular structure of [tpy^{tbu}phoH]^{0} obtained from single-crystal X-ray diffraction studies. All non-phenol H atoms removed for clarity. Crystals were grown by slow cooling a saturated hexane solution of the ligand. (**B**) Molecular structure of Cr(tpy^{tbu}pho)Cl$_2$ **1** obtained from single-crystal X-ray diffraction studies. Crystals were grown from slow evaporation of a DCM/MeCN mixture at room temperature. H atoms and MeCN molecule omitted for clarity. Blue = N, red = O, gray = C, green = Cl, maroon = Cr, white = H atoms; thermal ellipsoids at 50%. CCDC: 2086769-2086770.

Cyclic voltammetry (CV) experiments were performed on **1** in a solution of 0.1 M tetrabutylammonium hexafluorophosphate ($TBAPF_6$) in *N,N*-DMF. Under argon (Ar) saturation conditions **1** displays three redox features at potentials more negative than the ferrocenium/ferrocene (Fc^+/Fc) redox couple: $E_p = -1.46$ V, $E_{1/2} = -1.64$ V, and $E_{1/2} = -2.18$ V versus Fc^+/Fc (**Figure 3**, black and **Figure S6**), assigned as E_1^0, E_2^0, and E_3^0, respectively. A small wave is observed at $E_{1/2} = -1.85$ V, following the second reduction, which we propose relates to equilibria involving solvent displacement of a Cl^- bound to Cr. This proposal is supported by CV data obtained with tetrabutylammonium chloride (TBACl) present as a source of excess Cl^- anions (**Figures S7** and **S8**). Under Ar saturation conditions with added TBACl, only three reduction waves are observed and there is a shift towards more negative potentials for the first and second reductions of **1** relative to identical conditions in the absence of TBACl; the minor wave observed at $E_{1/2} = -1.85$ V vs Fc^+/Fc also disappears. These data suggest that overall, the complex undergoes three one-electron reduction events in the observed potential window, with two chloride-loss equilibria affecting the first two reductions, **Eq (1)-Eq (6)**, where L = $[tpy^{tbu}pho]^-$ and S = *N,N*-DMF. These assignments are supported by experiments described above, as well as DFT calculations, which show that the relevant equilibria depicted in **Eq (1)** and **Eq (3)** present reaction free energies of 0.9 kcal/mol ($K_{eq} = 0.22$) and −0.3 kcal/mol ($K_{eq} = 1.7$) as written, *vide infra* (**Figure S9**).

$[Cr(L)Cl_2]^0 + S \rightleftharpoons [Cr(L)Cl(S)]^+ + Cl^-$		**Eq (1)**
$[Cr(L)Cl(S)]^+ + e^- \rightleftharpoons [Cr(L)Cl(S)]^0$	E_1^0	**Eq (2)**
$[Cr(L)Cl(S)]^0 + S \rightleftharpoons [Cr(L)(S)_2]^+ + Cl^-$		**Eq (3)**
$[Cr(L)(S)_2]^+ + e^- \rightleftharpoons [Cr(L)(S)_2]^0$	E_2^0	**Eq (4)**
$[Cr(L)(S)_2]^0 \rightleftharpoons [Cr(L)(S)_2]^0 + S$		**Eq (5)**
$[Cr(L)S]^0 + e^- \rightleftharpoons [Cr(L)S]^-$	E_3^0	**Eq (6)**

Upon the addition of 0.1 M phenol (PhOH) under Ar saturation conditions, minimal shifts in the first two redox features of **1** are observed, but the third redox feature displays a slight

increase in current with some loss of reversibility (**Figure 3**, green). In the absence of an added proton donor under CO_2 saturation conditions, CV data indicates favorable CO_2 binding occurs: the third redox feature is observed to shift positively to $E_p = -2.13$ V versus Fc^+/Fc (**Figure 3**, red). The irreversibility observed at this feature and the appearance a second irreversible feature at a more negative potential (both with slight current increases) is consistent with limited aprotic CO_2 reduction activity occurring after CO_2 binding.

Under CO_2 saturation conditions in the presence of 0.1 M PhOH, a slight shift to positive potentials and large increase in current is observed which is consistent with the electrocatalytic CO_2 reduction reaction (CO2RR) mediated by **1** (**Figure 3**, blue). At 0.1 M PhOH cross-tracing is apparent by CV, which disappears with increased PhOH concentrations (**Figure S10**) and at higher scan rates (**Figure S11**). Additionally, similar CO2RR reactivity in *N,N*-DMF is observed with H_2O as a proton source instead of PhOH (**Figure S12**).

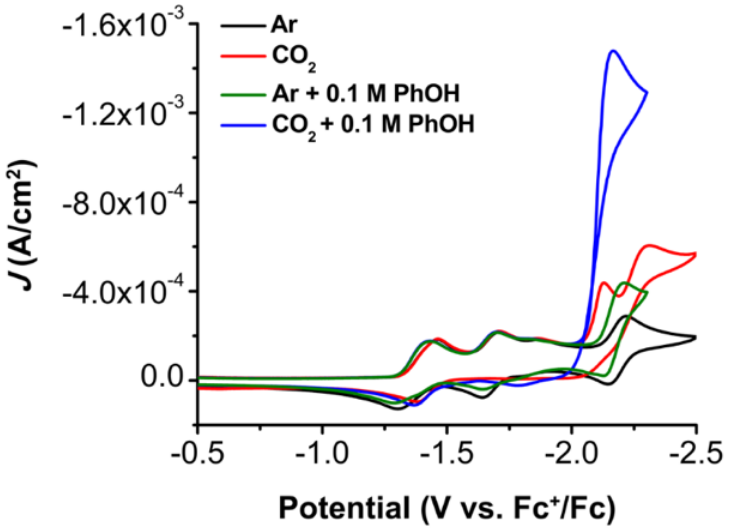

Figure 3. Comparison of CVs of 1.0 mM Cr(tpy^{tbu}pho)Cl_2 **1** under Ar and CO_2 saturation conditions with and without 0.1 M PhOH. Conditions: 0.1 M $TBAPF_6$/*N,N*-DMF; glassy carbon working electrode, glassy carbon rod counter electrode, Ag/AgCl pseudoreference electrode; referenced to Fc^+/Fc internal standard; 100 mV/s scan rate.

Variable concentration studies imply a first-order concentration dependence of catalytic current on **1** and CO_2 which saturates at modest concentrations when independently varied (**Figure S13** and **S14**, respectively). However, contrary to our previous report with Cr(^{tbu}dhbpy)Cl(H_2O), the catalytic current of the system with **1** is immediately saturated and does not increase with larger [PhOH] (**Figure S10**). This observation is distinct compared to the Cr(^{tbu}dhbpy)Cl(H_2O) system because it suggests that C–OH is no longer rate limiting in the catalytic mechanism with **1**.

Controlled potential electrolysis (CPE) experiments were performed at −2.3 V vs Fc^+/Fc with **1** and 0.6 M PhOH under CO_2 saturation conditions (**Figure S16** and **Table S3**). These results demonstrated a 93±7% Faradaic efficiency for CO (FE_{CO}) for **1** over 5 turnovers operating at an η of 260 mV with 2.66±0.05% H_2 detected (**Table 1**). Note that turnovers have been determined to show the catalytic nature of the process representing two electron equivalents of charge passed for one equivalent of **1** in solution and do not represent a measurement to complete loss of activity. No liquid products were detected in the post-bulk solution by ^{1}H NMR. The turnover frequency (TOF_{CPE}) derived from this electrolysis experiment is 1.82 s^{-1}, which is less than the TOF of 4.35 s^{-1} achieved by the bpy-based system during electrolysis.[18-19] The stability of the current during CPE is indicative of a stable catalytic system, which is supported by characterization of the post-CPE solution by UV-vis spectroscopy (**Figure S17**). To assess whether catalytic material had deposited during electrolysis, the working electrode was rinsed and used to perform a control electrolysis in the absence of **1** under otherwise identical conditions; non-quantifiable amounts of CO and significant H_2 was observed (**Figure S18** and **Table S4**). A control electrolysis experiment with PhOH under CO_2 saturation conditions in the absence of **1** and a freshly polished electrode showed the same product makeup as the rinse test (**Figure S19**).

Additionally, a CPE experiment was performed with 2% H_2O in *N,N*-DMF (v/v) as the proton source instead of PhOH (**Figure S20** and **Table S5**). With H_2O as a proton source in CPE experiments, **1** maintained excellent selectivity for CO, with a FE_{CO} of 93±4% over 8 turnovers with no quantifiable amount of H_2 detected and a TOF of 3.25 s^{-1} at an η of 470 mV (**Table 1**). A control electrolysis experiment with 2% H_2O in *N,N*-DMF showed no detectable CO and significant production of H_2 (**Figure S21**). Both TOF_{CPE} values are in good agreement with the TOF_{max} values of 4.37 and 13.7 s^{-1} calculated from CV data using the ratio of catalytic to Faradaic current at scan rates of 100 mV/s using PhOH and H_2O as the proton donor, respectively (**Figures 3** and **S12**; see SI).

Table 1. Results from CPE experiments under CO_2 saturation conditions.

Trial	Conditions	Proton Donor	Potential (V vs Fc^+/Fc)	FE_{CO}	FE_{H2}	TOF_{CPE} s^{-1}	η (V)	TON_{CO}
1	**1**+CO_2	0.6 M PhOH	−2.3	93±7	2.66±0.05	1.82	0.26	5.4
2	**1**+CO_2	1.0 M H_2O	−2.3	93±4	--	3.25	0.47	7.5
3	CO_2[a]	0.6 M PhOH	−2.3	--	--	--	n/a	--

[a] – performed with a used working electrode from trial 1 in the absence of the Cr-based precatalyst; [**1**] = $Cr(tpy^{tbu}pho)Cl_2$. Turnovers correspond to moles of electrons passed in coulometry studies divided by two to account for CO formation.

Mechanistic Insight via Computational (DFT) Analyses

In order to obtain additional insight, the reaction mechanism was interrogated by means of DFT calculations. CV data guided the initial investigation of the successive reduction events that the precatalyst undergoes to form the active species. Based on the proposal that solution equilibria involving the chloride ligands exists, five distinct redox events were examined for the overall three-electron reduction of complex **1**. Importantly, good correlation (R^2 = 0.94) between

experimental redox potentials and computational results is obtained, suggesting the level of theory was appropriate for modeling this system (see **Table S6** and **Figure S22**). Note, in the shorthand notation used in the ensuing discussion to describe these calculations, the [tpypho]$^{-}$ ligand has been eliminated for clarity and the other numbers are defined as follows $^{multiplicity}_{\#bound\ DMF}\mathbf{Cr}^{charge}$.

Unlike our previous study with the Cr(^{tbu}dhbpy)Cl(H_2O) catalyst,[18-19] the two-electron reduced species of Cr(tpy^{tbu}pho)Cl_2 is not reactive towards CO_2. Consistent with experimental observations, it is the third overall reduction event (exp. $E_{1/2}$ = −2.18 V vs Fc^+/Fc) that produces an overall monoanionic species capable of binding and activating CO_2. Therefore, the active species of both catalysts have analogous overall charge (−1) and formal metal oxidation state (high-spin Cr(II)), while differing in the number of ligand-centered reduction events (one for ^{tbu}dhbpy, two for tpy^{tbu}pho). In order to experimentally support this assignment, we synthesized a zinc (Zn) complex in the same ligand framework, [Zn(tpy^{tbu}pho)][OTf] (see **SI**, **Figure S25**). The CVs of this Zn complex reveal two quasi-reversible one-electron redox features at slightly more negative potentials than the second and third redox features observed for **1** (**Figure S26**). In this potential range, Zn(II) is expected to remain redox-inert and therefore the absence of a third reduction feature for the Zn-based control complex is consistent with the proposal that two primarily ligand-based reductions occur during the pre-catalytic activation of **1**. The negative shift of the redox events for the Zn-based complex relative to **1** can be attributed to the absence of electronic coupling between the ligand and the d^{10} Zn(II) center, in comparison to the high-spin d^4 Cr(II) center.

As a consequence of this increased ligand-based redox activity, the overall spin manifold is necessarily different between the tpy- and bpy-based complexes: while S = 3/2 was found to be

the preferential configuration for [Cr(II)(^{tbu}dhbpy$^{\bullet}$)]$^{-}$, the lowest-energy spin configuration for the active species for [Cr(II)(tpy^{tbu}pho$^{\bullet\bullet}$)]$^{-}$ was an overall triplet (S = 1), with a terpyridine triplet diradical antiferromagnetically coupled to a high-spin Cr(II) center (**Figures 4A** and **S23A**). This finding is in good agreement with previous studies of terpyridine-containing electrocatalysts.[23-24] Notably, the pentacoordinate solvent adduct $^{3}_{1}\mathbf{Cr}^{-1}$ and tetracoordinate species $^{3}_{0}\mathbf{Cr}^{-1}$ of the tpy-based catalyst are almost equally stable (ΔG = 0.2 kcal/mol), the former being the lowest-energy configuration. Quintet ($^{5}_{0}\mathbf{Cr}^{-1}$) and septet ($^{7}_{0}\mathbf{Cr}^{-1}$) configurations were found at 3.0 and 6.8 kcal/mol above $^{3}_{1}\mathbf{Cr}^{-1}$, respectively.

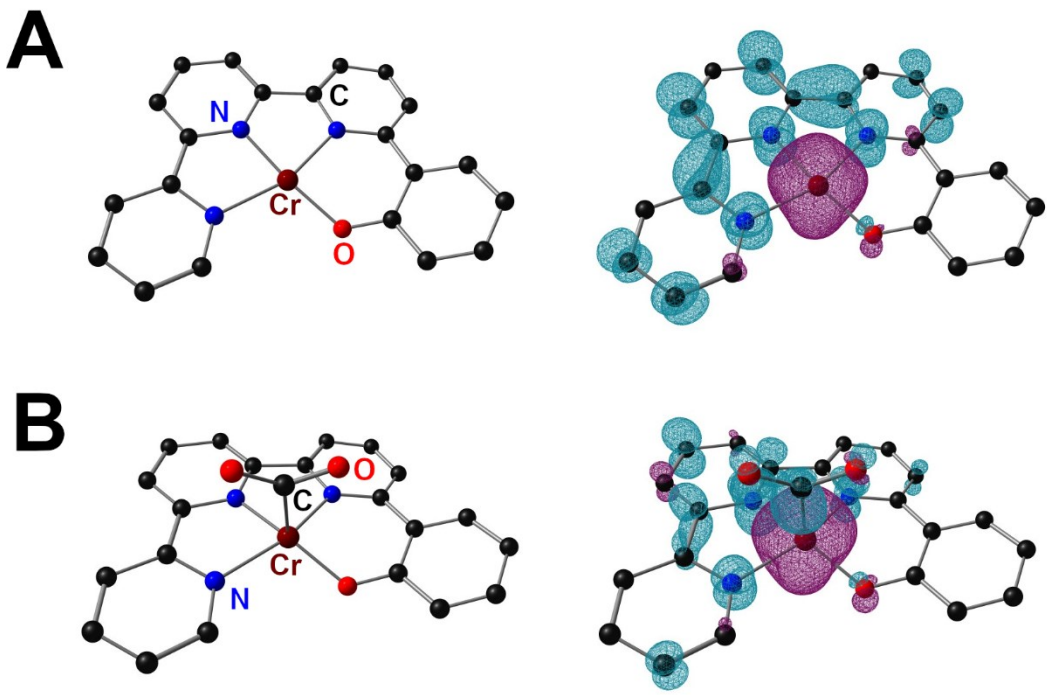

Figure 4. Molecular geometry and spin density plots of $^{3}_{0}\mathbf{Cr}^{-1}$ (**A**) and $^{3}_{0}\mathbf{Cr(CO_2)}^{-1}$ (**B**). For clarity, tbu groups and H atoms have been omitted.

From $^{3}_{1}\mathbf{Cr}^{-1}$, the lowest-energy configuration for the transition state to bind CO_2 (no axial DMF, **Figures S23 and S24**) and the corresponding adduct (**Figure 4B** and **S23B**) were located

in the S = 1 surface. The barrier for this catalyst was found to be higher ($^{3}_{0}\mathbf{TS1}^{-1}$, +12.2 kcal/mol) (**Figure 5**) than that located for CO_2 binding for the dhbpy counterpart (+10.0 kcal/mol). Interestingly, $^{3}_{0}\mathbf{TS1}^{-1}$ presents a Cr−C bond distance of 2.35 Å, much shorter than the 2.64 Å found for the corresponding TS of the dhbpy system. This can be rationalized by analyzing the electronic structure of these species: for the dhbpy catalyst system, one of the two electrons that form the Cr−C bond is highly delocalized in a bpy-centered, metal-mixed π* orbital in the TS geometry (see reference[19]), conversely, for $^{3}_{0}\mathbf{TS1}^{-1}$ both electrons have predominantly Cr−C σ-bond character (**Figure S24**). Furthermore, for the terpyridine-based catalyst CO_2 binding is exergonic ($^{3}_{0}\mathbf{Cr(CO_2)}^{-1}$, −1.9 kcal/mol), in stark contrast with the endergonic binding calculated previously for the dhbpy system (+4.7 kcal/mol, **Figure S27**) and in good agreement with CV data for both systems. The electronic structure of the CO_2 adduct confirms the partial charge transfer from the reduced ligand: $^{3}_{0}\mathbf{Cr(CO_2)}^{-1}$ presents a singly reduced tpy fragment (**Figure 4B**). The barrier for the thermodynamically favorable (−15.8 kcal/mol) formation of a metal hydride was located at +20.7 kcal/mol above $^{3}_{1}\mathbf{Cr}^{-1}$, in agreement with the observed nearly quantitative kinetic selectivity for CO (**Figure S27**).

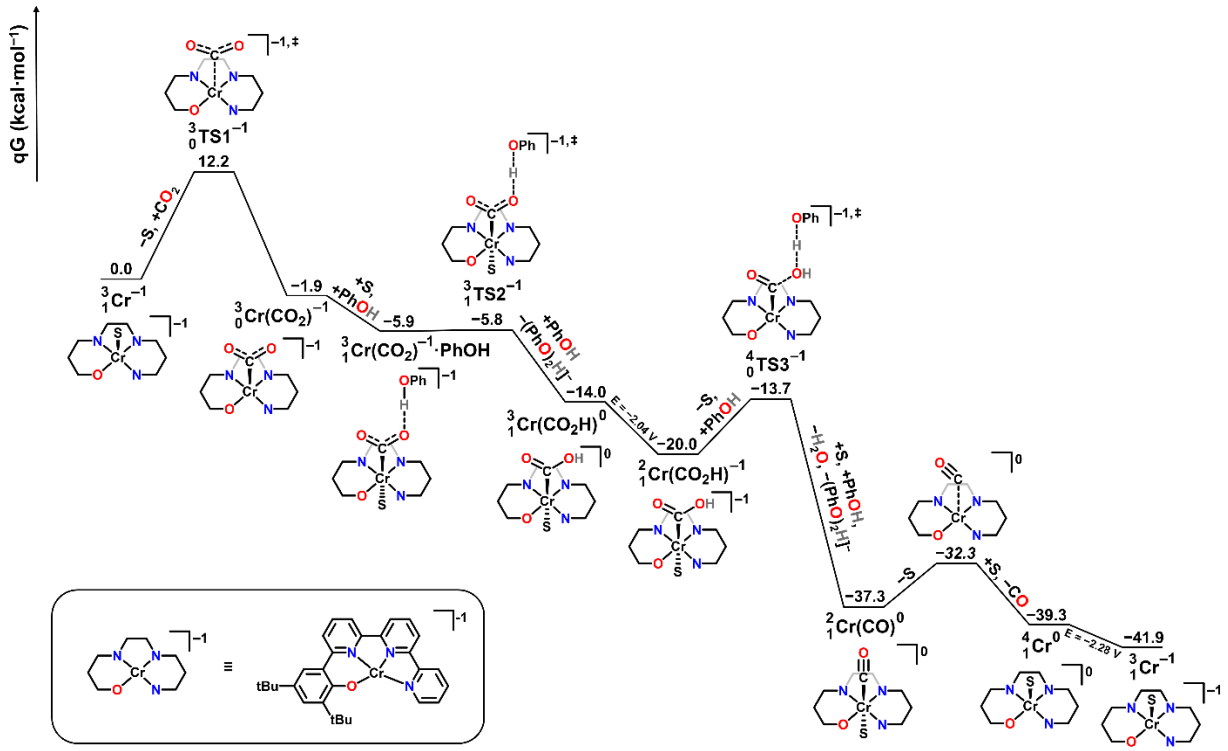

Figure 5. Free energy profile of the electrocatalytic CO2RR cycle for **1**. Precatalyst reduction steps are omitted for clarity. S indicates a solvent adduct of *N,N*-DMF; procedure for the estimation of the barrier for CO release is described in the Supporting Information.

PhOH favorably binds to $^{3}_{0}\mathbf{Cr(CO_2)}^{-1}$ to give $^{3}_{1}\mathbf{Cr(CO_2)\cdot PhOH}^{-1}$ at −5.9 kcal/mol relative to $^{3}_{1}\mathbf{Cr}^{-1}$, from which proton transfer has a barrier of only 0.1 kcal/mol ($^{3}_{1}\mathbf{TS2}^{-1}$, **Figure 6A**) and is thermodynamically favorable by 12.1 kcal/mol relative to $^{3}_{0}\mathbf{Cr(CO_2)}^{-1}$ (PhOH homoconjugation in *N,N*-DMF and *N,N*-DMF binding to the product were taken into account[19, 29]). The calculated reduction potential for the neutral six-coordinate hydroxycarbonyl complex $^{3}_{1}\mathbf{Cr(CO_2H)}^{0}$ is −2.12 V, leading to the doublet species $^{2}_{1}\mathbf{Cr(CO_2H)}^{-1}$ at potentials below the experimentally observed $E_{cat/2}$. The electronic structure of $^{2}_{1}\mathbf{Cr(CO_2H)}^{-1}$ is comprised of a doubly reduced, triplet diradical terpyridine and a high-spin Cr(III) center (**Figure S28**). Hydrogen bonding of PhOH to $^{2}_{1}\mathbf{Cr(CO_2H)}^{-1}$ to form $^{2}_{1}\mathbf{Cr(CO_2H)\cdot PhOH}^{-1}$ is slightly uphill (+2.3

kcal/mol). Importantly, the quartet configuration of the PhOH adduct, $^{4}_{0}\mathbf{Cr(CO_2H)\cdot PhOH}^{-1}$, becomes isoenergetic (just 0.2 kcal/mol above $^{2}_{1}\mathbf{Cr(CO_2H)\cdot PhOH}^{-1}$) upon DMF release, giving access to the lowest-energy C−OH bond cleavage transition state for this system ($^{4}_{0}\mathbf{TS3}^{-1}$, **Figure 6B**) at only +6.3 kcal/mol above $^{2}_{1}\mathbf{Cr(CO_2H)}^{-1}$ and free PhOH (**Figure 5**). By comparison the transition state for the doublet solvento species $^{2}_{1}\mathbf{TS3}^{-1}$ lies higher in energy at +10.6 kcal/mol above $^{2}_{1}\mathbf{Cr(CO_2H)}^{-1}$ and free phenol. C–OH bond cleavage is therefore both thermodynamically favorable (−17.4 kcal/mol) and does not appear to be rate-limiting. Notably, this reaction barrier is much lower than the corresponding C−OH bond cleavage in the dhbpy system (+10.4 kcal/mol).

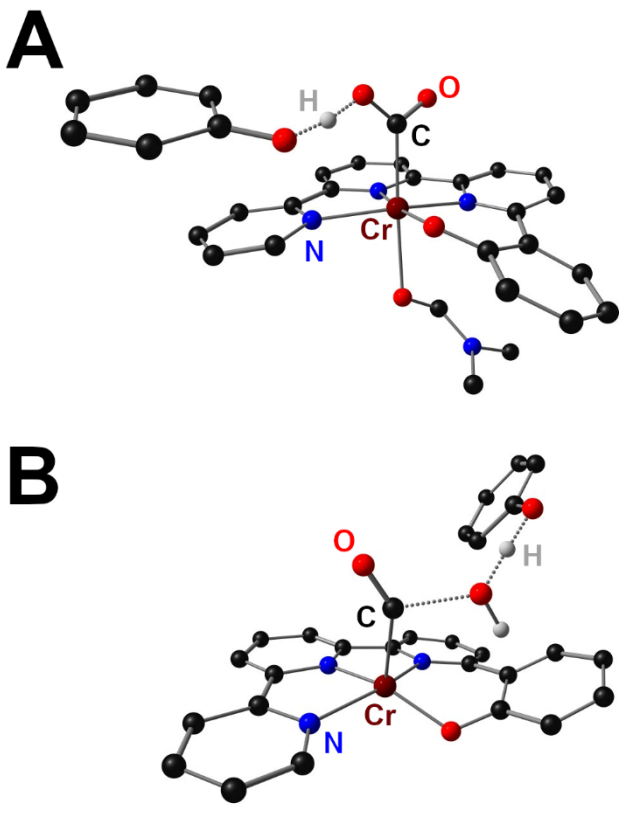

Figure 6. Molecular geometries of $^{3}_{1}\mathbf{TS2}^{-1}$ (**A**) and $^{4}_{0}\mathbf{TS3}^{-1}$ (**B**). For clarity, tbu groups and H atoms have been omitted.

The lowest-energy spin configuration of the metal carbonyl formed from C–OH bond cleavage is the doublet ($^{2}_{1}$**Cr(CO)** ^{0}), arising from antiferromagnetically coupled electrons delocalized through the terpyridine backbone and the Cr−CO bond (**Figure S29**), from which we propose CO dissociation is facile and irreversible (**Figure S30**).[18-19, 30-31] It is worth noting that while doublet spin configurations are preferred for the reactants and products of the C–OH bond cleavage step, the lowest energy transition state is a quartet. The spin change that occurs in the isoenergetic dissociation (+0.2 kcal/mol) of DMF from $^{2}_{1}$**Cr(CO$_2$H)·PhOH**$^{-1}$ to generate the five-coordinate $^{4}_{0}$**Cr(CO$_2$H)·PhOH**$^{-1}$ reflects the transfer of an electron from a primarily ligand centered orbital to a molecular orbital which is distributed between the Cr and tpy fragments (comparing **Figures S31** and **S32**). In the corresponding transition states for each spin manifold, anti-bonding character builds up in the C–OH bond in $^{4}_{0}$**TS3**$^{-1}$ (**Figure S33**, while the comparable frontier orbitals of $^{2}_{1}$**TS3**$^{-1}$ show significant π-bonding between Cr and C (**Figure S34**), reminiscent of the nascent carbonyl group. In other words, solvent dissociation allows electron transfer from tpy into the Cr orbitals relevant to bond cleavage, manifesting in a lower energy pathway as these orbitals become more reactive. While this electron transfer does not manifest in a formal shift from a Cr(III)(tpy$^{\bullet\bullet 2-}$) configuration to Cr(II)(tpy$^{\bullet-}$), it can be thought of an intermediate scenario along this continuum.

Alternate spin manifolds were considered for all intermediates and transition states but were found to be higher in energy (see XYZ file). The relative energetic positioning of possible spin manifolds in the catalytic cycle also showed good agreement between the hybrid B3LYP

functional[32-35] and the meta-GGA revised TPSS functional,[36-37] indicating the method was appropriate for these assignments (**Table S7**).[38]

Discussion

It is striking that the tpy-based Cr complex **1** largely achieves comparable activity and selectivity at similar overpotentials to the bpy-based catalyst we have reported previously. Unlike the bpy-based catalyst, however, complex **1** binds CO_2 in the absence of a proton donor (**Figure 3**, red). Computational studies relevant to CO_2 binding suggest that, in comparison to the bpy-based complex,[18-19] at the TS geometry the electrons forming the incipient Cr–C bond are relatively more localized on the metal and sigma-based, which could contribute to the relatively heightened barrier for **1** in comparison to the bpy-based complex. Indeed, this is consistent with the need for charge reorganization from the doubly reduced tpy fragment to Cr being a key component. The formation of the CO_2 adduct $[Cr(tpy^{tbu}pho^{\bullet})(\eta^1\text{-}CO_2)]^-$ is also significantly exergonic, in contrast to the endergonic formation of $[Cr(^{tbu}dhbpy)(\eta^1\text{-}CO_2)]^-$.[18-19] This trend is consistent with differences in operating potential: the catalytically relevant reduction potential of complex **1** ($E_{1/2}$ = −2.18 V) is 0.23 V more negative than the bpy-based complex ($E_{1/2}$ = −1.95 V).

The facile access to σ-basic character at Cr makes $[Cr(II)(tpy^{tbu}pho^{\bullet\bullet})(DMF)]^-$ more adept at interacting with the added proton donor PhOH than $[Cr(II)(^{tbu}dhbpy^{\bullet})]^-$, which presents relatively more π-basic character. In CV studies with added PhOH under Ar saturation (**Figure 3**, green), a loss of reversibility occurs at the third reduction, consistent with an interaction between the Cr center and the proton donor. Conversely, the bpy-based Cr catalyst exhibited no comparable activity with added PhOH.[18-19] DFT calculations show that the difference in transition state energy (ΔTS) between the barrier for protonation and CO_2 binding narrows across these two catalysts (ΔTS is 8.5 kcal/mol for $[Cr(II)(tpy^{tbu}pho^{\bullet\bullet})(DMF)]^-$, versus 20.2 kcal/mol for

[Cr(II)(^{tbu}dhbpy$^{\bullet}$)]$^{-}$,[19] **Figure S27**), consistent with the experimentally observed reactivity trends. Further, hydride formation from [Cr(II)(^{tbu}dhbpy$^{\bullet}$)]$^{-}$ is exergonic (−7.2 kcal/mol), whereas comparable hydride formation from [Cr(II)(tpy^{tbu}pho$^{\bullet\bullet}$)(DMF)]$^{-}$ is even more thermodynamically favored, –15.8 kcal/mol. The difference is apparent under electrocatalytic conditions: **1** produces minor amounts of H_2, **Table 1**.

An additional consequence of the more negative potentials required for CO_2 binding by **1** appears to be relatively lower barriers for protonation to generate and protonate a hydroxycarbonyl intermediate (Cr–CO_2H) than those for the bpy-based analogue. Experimentally, saturation of the electrocatalytic current with added proton donor occurs at low concentrations for **1**, whereas a kinetic rate dependence was previously assessed for the bpy-based analogue. Computations again reflect these reactivity trends, suggesting that CO_2 binding is the rate-determining step for complex **1**, as opposed to the bpy-based catalyst, where C–OH bond cleavage was determined to be the rate-determining step.

Formation of a second key diradical state in the reduced ligand occurs again in [Cr(II)(tpy^{tbu}pho$^{\bullet\bullet}$)(η^1-CO_2H)]$^{-}$ (S = 3/2), which precedes C–OH bond cleavage. During the formation of the Cr carbonyl and water co-products, one of these ligand-based unpaired electrons is transferred into the π-back-bonding scaffold of the forming CO ligand. For [Cr(II)(^{tbu}dhbpy$^{\bullet}$)(η^1-CO_2H)]$^{-}$ (S = 1), a similar reaction pathway occurs, however, the barrier is relatively more significant and defines the rate of the process.[18-19] It is noteworthy that the increased redox-activity of tpy assists in diminishing the barrier of this chemical reaction step, since two charge equivalents are coupled to Cr and available for transfer, rather than one. Although excellent agreement between theory and experiment have been achieved here, we encourage the use of higher-levels of theory for obtaining *a priori* predictive insight on the electronic structure of metal complexes whose spin

manifolds might contain strongly coupled ligand and metal components to better assess the possibility of multiconfigurational active spaces.[39]

Conclusions

We report a new Cr-based electrocatalyst for the reduction of CO_2 to CO. Selective and stable Cr-based catalysts are underrepresented for the CO2RR.[4-6] Indeed, there are limited overall examples of the Cr/Mo/W triad showing either electrochemical or electrocatalytic activity.[10-17] By expanding the polypyridyl core of the ligand, the ligand must be reduced twice to initiate the catalytic cycle, producing an active state which is best described as $[Cr(II)(tpy^{tbu}pho^{\bullet\bullet})]^{-}$ (S = 1). The formation of a ligand-based diradical occurs again later in the catalytic cycle, when the intermediate prior to C–OH bond cleavage $^{2}_{1}\mathbf{Cr(CO_2H)}^{-1}$ is generated, demonstrating that coupling between the tpy-based ligand and Cr center alters the rate-determining step of the catalytic cycle. These results suggest that the ligand design principles used to develop selective, active, and stable late transition metal catalysts for the CO2RR can be applied to metals much earlier in the transition metal series to create new categories of carbonyl ligand-free catalysts.

ASSOCIATED CONTENT

Supporting Information. Additional Material and Methods, CV, UV-vis, NMR, electrochemical data, and computational coordinates are included as supporting information. Crystal data has been deposited with the CCDC: 2086769-2086770.

AUTHOR INFORMATION

Corresponding Author. * - machan@virginia.edu

Funding Sources

University of Virginia.

ACKNOWLEDGMENT

This research was supported by the U.S. Department of Energy, Office of Science, Office of Basic Energy Sciences, Catalysis Science Program, under Award DE-SC0022219. Single crystal X-ray diffraction experiments were performed on a diffractometer at the University of Virginia funded by the NSF-MRI program (CHE-2018870). We acknowledge the University of Virginia for maintenance and support with the Rivanna High-Performance Computing Center.

NOTES

A previous version of this manuscript has been deposited on a preprint server.[40]

References:

1. DuBois, D. L., Development of Molecular Electrocatalysts for Energy Storage. *Inorg. Chem.* **2014,** *53* (8), 3935-3960.
2. Das, B.; Thapper, A.; Ott, S.; Colbran, S. B., Structural features of molecular electrocatalysts in multi-electron redox processes for renewable energy – recent advances. *Sustain. Energy Fuels* **2019,** *3* (9), 2159-2175.
3. IPCC *Global Warming of 1.5°C. An IPCC Special Report*; World Meterological Organization: Geneva, Switzerland, 2018.
4. Jiang, C.; Nichols, A. W.; Machan, C. W., A look at periodic trends in d-block molecular electrocatalysts for CO_2 reduction. *Dalton Trans.* **2019,** *48*, 9454-9468.
5. Francke, R.; Schille, B.; Roemelt, M., Homogeneously Catalyzed Electroreduction of Carbon Dioxide—Methods, Mechanisms, and Catalysts. *Chem. Rev.* **2018,** *118* (9), 4631-4701.
6. Kinzel, N. W.; Werlé, C.; Leitner, W., Transition Metal Complexes as Catalysts for the Electroconversion of CO_2: An Organometallic Perspective. *Angew. Chem. Int. Ed.* **2021,** *60* (21), 11628-11686.
7. West, N. M.; Miller, A. J. M.; Labinger, J. A.; Bercaw, J. E., Homogeneous syngas conversion. *Coord. Chem. Rev.* **2011,** *255* (7), 881-898.
8. Kalck, P.; Le Berre, C.; Serp, P., Recent advances in the methanol carbonylation reaction into acetic acid. *Coord. Chem. Rev.* **2020,** *402*, 213078.
9. Hood, D. M.; Johnson, R. A.; Carpenter, A. E.; Younker, J. M.; Vinyard, D. J.; Stanley, G. G., Highly active cationic cobalt(II) hydroformylation catalysts. *Science* **2020,** *367* (6477), 542-548.
10. Clark, M. L.; Grice, K. A.; Moore, C. E.; Rheingold, A. L.; Kubiak, C. P., Electrocatalytic CO_2 reduction by M(bpy-R)($CO)_4$ (M = Mo, W; R = H, *t*Bu) complexes. Electrochemical, spectroscopic, and computational studies and comparison with group 7 catalysts. *Chem. Sci.* **2014,** *5* (5), 1894-1900.
11. Ramos Sende, J. A.; Arana, C. R.; Hernandez, L.; Potts, K. T.; Keshevarz-K, M.; Abruna, H. D., Electrocatalysis of CO_2 Reduction in Aqueous Media at Electrodes Modified with

Electropolymerized Films of Vinylterpyridine Complexes of Transition Metals. *Inorg. Chem.* **1995,** *34* (12), 3339-3348.
12. Pickett, C. J.; Pletcher, D., Electrochemical reduction of Group 6 metal hexacarbonyls in aprotic solvents. *J. Chem. Soc., Dalton Trans.* **1976,** (8), 749-752.
13. Maia, L. B.; Fonseca, L.; Moura, I.; Moura, J. J. G., Reduction of Carbon Dioxide by a Molybdenum-Containing Formate Dehydrogenase: A Kinetic and Mechanistic Study. *J. Am. Chem. Soc.* **2016,** *138* (28), 8834-8846.
14. Tory, J.; Setterfield-Price, B.; Dryfe, R. A. W.; Hartl, F., [$M(CO)_4$(2,2′-bipyridine)] (M=Cr, Mo, W) Complexes as Efficient Catalysts for Electrochemical Reduction of CO_2 at a Gold Electrode. *ChemElectroChem* **2015,** *2* (2), 213-217.
15. Grice, K. A.; Saucedo, C., Electrocatalytic Reduction of CO_2 by Group 6 $M(CO)_6$ Species without "Non-Innocent" Ligands. *Inorg. Chem.* **2016,** *55* (12), 6240-6246.
16. Neri, G.; Donaldson, P. M.; Cowan, A. J., The Role of Electrode–Catalyst Interactions in Enabling Efficient CO_2 Reduction with Mo(bpy)$(CO)_4$ As Revealed by Vibrational Sum-Frequency Generation Spectroscopy. *J. Am. Chem. Soc.* **2017,** *139* (39), 13791-13797.
17. Mouchfiq, A.; Todorova, T. K.; Dey, S.; Fontecave, M.; Mougel, V., A bioinspired molybdenum–copper molecular catalyst for CO_2 electroreduction. *Chem. Sci.* **2020,** *11* (21), 5503-5510.
18. Hooe, S. L.; Dressel, J. M.; Dickie, D. A.; Machan, C. W., Highly Efficient Electrocatalytic Reduction of CO_2 to CO by a Molecular Chromium Complex. *ACS Catal.* **2020,** *10* (2), 1146-1151.
19. Moreno, J. J.; Hooe, S. L.; Machan, C. W., DFT Study on the Electrocatalytic Reduction of CO_2 to CO by a Molecular Chromium Complex. *Inorg. Chem.* **2021,** *60* (6), 3635-3650.
20. Hooe, S. L.; Moreno, J. J.; Reid, A. G.; Cook, E. N.; Machan, C. W., Mediated Inner-Sphere Electron Transfer Induces Homogeneous Reduction of CO_2 via Through-Space Electronic Conjugation**. *Angew. Chem. Int. Ed.* **2022,** *61* (1), e202109645.
21. Benson, E. E.; Sampson, M. D.; Grice, K. A.; Smieja, J. M.; Froehlich, J. D.; Friebel, D.; Keith, J. A.; Carter, E. A.; Nilsson, A.; Kubiak, C. P., The Electronic States of Rhenium Bipyridyl Electrocatalysts for CO_2 Reduction as Revealed by X-ray Absorption Spectroscopy and Computational Quantum Chemistry. *Angew. Chem., Int. Ed.* **2013,** *52* (18), 4841-4844.
22. Smieja, J. M.; Benson, E. E.; Kumar, B.; Grice, K. A.; Seu, C. S.; Miller, A. J. M.; Mayer, J. M.; Kubiak, C. P., Kinetic and structural studies, origins of selectivity, and interfacial charge transfer in the artificial photosynthesis of CO. *Proc. Natl. Acad. Sci.* **2012,** *109* (39), 15646-15650.
23. Derrick, J. S.; Loipersberger, M.; Chatterjee, R.; Iovan, D. A.; Smith, P. T.; Chakarawet, K.; Yano, J.; Long, J. R.; Head-Gordon, M.; Chang, C. J., Metal–Ligand Cooperativity via Exchange Coupling Promotes Iron- Catalyzed Electrochemical CO_2 Reduction at Low Overpotentials. *J. Am. Chem. Soc.* **2020,** *142* (48), 20489-20501.
24. Loipersberger, M.; Cabral, D. G. A.; Chu, D. B. K.; Head-Gordon, M., Mechanistic Insights into Co and Fe Quaterpyridine-Based CO_2 Reduction Catalysts: Metal–Ligand Orbital Interaction as the Key Driving Force for Distinct Pathways. *Journal of the American Chemical Society* **2021,** *143* (2), 744-763.
25. Keith, J. A.; Grice, K. A.; Kubiak, C. P.; Carter, E. A., Elucidation of the Selectivity of Proton-Dependent Electrocatalytic CO_2 Reduction by fac-Re(bpy)$(CO)_3$Cl. *J. Am. Chem. Soc.* **2013,** *135* (42), 15823-15829.

26. Riplinger, C.; Sampson, M. D.; Ritzmann, A. M.; Kubiak, C. P.; Carter, E. A., Mechanistic Contrasts between Manganese and Rhenium Bipyridine Electrocatalysts for the Reduction of Carbon Dioxide. *J. Am. Chem. Soc.* **2014,** *136* (46), 16285-16298.
27. Cometto, C.; Chen, L.; Lo, P.-K.; Guo, Z.; Lau, K.-C.; Anxolabéhère-Mallart, E.; Fave, C.; Lau, T.-C.; Robert, M., Highly Selective Molecular Catalysts for the CO_2-to-CO Electrochemical Conversion at Very Low Overpotential. Contrasting Fe vs Co Quaterpyridine Complexes upon Mechanistic Studies. *ACS Catal.* **2018,** *8* (4), 3411-3417.
28. Newkome, G. R.; Hager, D. C.; Kiefer, G. E., Chemistry of heterocyclic compounds. Part 119. Synthesis of halogenated terpyridines and incorporation of the terpyridine nucleus into a polyetheral macrocycle. *J. Org. Chem.* **1986,** *51* (6), 850-853.
29. Nielsen, M. F.; Hammerich, O.; Rise, F.; Gogoll, A.; Undheim, K.; Wang, D. N.; Christensen, S. B., The Effect of Hydrogen Bonding between Methyl-Substituted Phenols and Dipolar Aprotic Solvents on the Rate Constants for. *Acta. Chem. Scan.* **1992,** *46*, 883-896.
30. Labrum, N. S.; Chen, C.-H.; Caulton, K. G., A bis-Pyrazolate Pincer on Reduced Cr Deoxygenates CO_2: Selective Capture of the Derived Oxide by Cr^{II}. *Chem. - Eur. J.* **2019,** *25* (33), 7935-7940.
31. Perrotin, P.; Shapiro, P. J.; Williams, M.; Twamley, B., In Search of a Versatile Pathway to ansa-Chromocene Complexes. Synthesis and Characterization of the Highly Unstable ansa-Chromocene Carbonyl Complex $Me_2C(C_5H_4)_2CrCO$. *Organometallics* **2007,** *26* (7), 1823-1826.
32. Becke, A. D., Density-functional thermochemistry. III. The role of exact exchange. *J. Chem. Phys.* **1993,** *98* (7), 5648-5652.
33. Vosko, S. H.; Wilk, L.; Nusair, M., Accurate spin-dependent electron liquid correlation energies for local spin density calculations: a critical analysis. *Can. J. Phys.* **1980,** *58* (8), 1200-1211.
34. Lee, C.; Yang, W.; Parr, R. G., Development of the Colle-Salvetti correlation-energy formula into a functional of the electron density. *Phys. Rev. B* **1988,** *37* (2), 785-789.
35. Stephens, P. J.; Devlin, F. J.; Chabalowski, C. F.; Frisch, M. J., Ab Initio Calculation of Vibrational Absorption and Circular Dichroism Spectra Using Density Functional Force Fields. *J. Phys. Chem.* **1994,** *98* (45), 11623-11627.
36. Perdew, J. P.; Ruzsinszky, A.; Csonka, G. I.; Constantin, L. A.; Sun, J., Workhorse Semilocal Density Functional for Condensed Matter Physics and Quantum Chemistry. *Phys. Rev. Lett.* **2009,** *103* (2), 026403.
37. Perdew, J. P.; Ruzsinszky, A.; Csonka, G. I.; Constantin, L. A.; Sun, J., Erratum: Workhorse Semilocal Density Functional for Condensed Matter Physics and Quantum Chemistry [Phys. Rev. Lett. 103, 026403 (2009)]. *Phys. Rev. Lett.* **2011,** *106* (17), 179902.
38. Neale, S. E.; Pantazis, D. A.; Macgregor, S. A., Accurate computed spin-state energetics for Co(III) complexes: implications for modelling homogeneous catalysis. *Dalton Trans.* **2020,** *49* (19), 6478-6487.
39. Keith, J. A.; Vassilev-Galindo, V.; Cheng, B.; Chmiela, S.; Gastegger, M.; Müller, K.-R.; Tkatchenko, A., Combining Machine Learning and Computational Chemistry for Predictive Insights Into Chemical Systems. *Chem. Rev.* **2021,** *121* (16), 9816-9872.
40. Reid, A. G.; Hooe, S. L.; Moreno, J. J.; Dickie, D. A.; Charles, W. M., Homogeneous Electrocatalytic Reduction of CO_2 by a CrN_3O Complex: Electronic Coupling with Redox-Active Terpyridine Fragment Favors Selectivity for CO. *ChemRxiv* **2022**, 10.26434/chemrxiv-2021-lplvt-v2.

TOC:

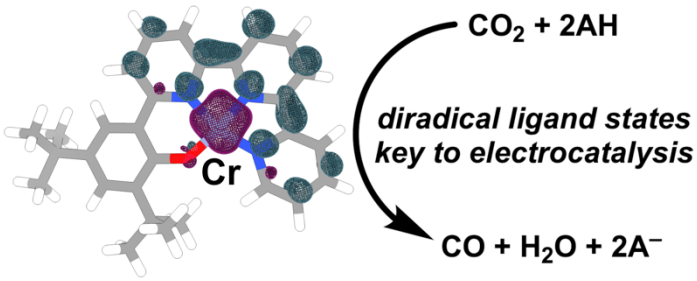

A new terpyridine-based CrN_3O catalyst reduces CO_2 to CO with almost quantitative selectivity. Computational and mechanistic analyses indicate that the decrease in intrinsic ligand charge and increase in ligand redox activity relative to the bipyridine-based analogue result in stronger electronic coupling between the ligand and metal center. This interaction enhances the rate of protonation and subsequent C–OH bond cleavage, resulting in CO_2 binding becoming the rate-determining step of catalysis.